Nano Research 2015, 8(9): 2871–2880
DOI 10.1007/s12274-015-0792-0
Research Article
ISSN 1998-0124
CN 11-5974/O4

Ag nanoparticle/polymer composite barcode nanorods

Hongxu Chen[1], Tieqiang Wang[2], Huaizhong Shen[1], Wendong Liu[1], Shuli Wang[1], Kun Liu[1], Junhu Zhang[1] (✉), and Bai Yang[1]

[1] *State Key Laboratory of Supramolecular Structure and Materials, College of Chemistry, Jilin University, Changchun 130012, China*
[2] *Department of Chemistry, College of Sciences, Northeastern University, Shenyang 110004, China*

Received: 13 January 2015
Revised: 7 April 2015
Accepted: 14 Arpil 2015

KEYWORDS
colloidal lithography,
nanoparticle/polymer composites,
nanorod,
barcode

ABSTRACT

We demonstrate a facile method combining colloidal lithography, selective ion-exchange, and the *in situ* reduction of Ag ions (Ag^+) for the fabrication of multi-segmented barcode nanorods. First, polymer multilayer films were prepared by spin-coating alternating thin films of polystyrene and polyacrylic acid (PAA), and then multi-segmented polymer nanorods were fabricated via reactive ion etching with colloidal masks. Second, Ag nanoparticles (Ag NPs) were incorporated into the PAA segments by an ion exchange and the *in situ* reduction of the Ag^+. The selective incorporation of the Ag NPs permitted the modification of the specific bars of the nanorods. Lastly, the Ag NP/polymer composite nanorods were released from the substrate to form suspensions for further coding applications. By increasing the number of segments and changing the length of each segment in the nanorods, the coding capacity of nanorods was improved. More importantly, this method can easily realize the density tuning of Ag NPs in different segments of a single nanorod by varying the composition of the PAA segments. We believe that numerous other coded materials can also be obtained, which introduces new approaches for fabricating barcoded nanomaterials.

1 Introduction

Encoded nanomaterials, which have a large number of readily distinguishable barcode patterns, are used in many fields, including cryptography, computational science, brand protection, the covert tracking of material goods and personnel, and labeling for biological and chemical diagnostics [1–6]. They can be dispersed or hidden in a variety of media owing to their small size, and their chemical and physical properties can be rationally designed in a variety of ways [7–15]. Widespread application of the barcoded nanomaterials requires a high coding capacity (i.e., a large number of recognizable and reproducible signatures), low-cost and large-scale barcode production, and an accurate, portable, and rapid non-contact detection system with a high identification accuracy [3]. To satisfy these demands, many barcoded nanomaterials have been

Address correspondence to zjh@jlu.edu.cn

developed [1–6, 16–27]. Among them, nanowires are particularly attractive because of their high aspect ratio and ability to generate multiple outer surfaces. Accordingly, template-assisted electrochemical synthesis is extremely useful for preparing a wide range of metallic, semiconductor, and polymeric nanowires [1–6, 16, 24–25]. The attractive synthesis and properties of nanowires make them extremely attractive for designing effective barcoded materials with a high coding capacity and reproducible signatures.

Like nanowires, barcode nanorod materials have received considerable attention owing to their low cost, high throughput, high volume, ease of production, and ability to generate multiple outer surfaces [14, 18, 23]. Barcode nanorods have many important applications and have been used in many fields. For example, Liu et al. reported the synthesis of luminescent crystals based on hexagonal-phase $NaYF_4$ upconversion microrods and demonstrated the use of the as-synthesized multicolor microrods as barcodes for anti-counterfeiting applications [28]; Keating and Natan et al. also synthesized multi-metal microrods intrinsically encoded with sub-micrometer stripes. They demonstrated that simultaneous immunoassays could be performed on the rods and that the reflectivity image was sufficient for the identification of the capture chemistry on a given particle [7]. Tok et al. employed metallic nanowires (both magnetic and nonmagnetic) as novel platforms for multiplex immunoassays [14]. Mirkin et al. highlighted recent advances in the synthesis of multi-segmented one-dimensional nanorods and nanowires with metal, semiconductor, polymer, molecular, and even gapped components, discussing the applications of these multicomponent nanomaterials in magnetism, self-assembly, electronics, biology, catalysis, and optics [23].

Noble-metal materials, which can effectively improve the coding capacity and signal output, have also been utilized in a variety of applications [29, 30]. Template synthesis is the most widely used method for the synthesis of multicomponent metal nanorods and nanowires, but metals cannot be electrochemically deposited without a hard template. There have been few reports on the synthesis of multi-segmented metallic nanostructures without hard templates, despite the fact that this approach is advantageous with regard to the structural variety and controllability. Thus, we focus on multi-segmented nanorods prepared with a controllable size via simple and inexpensive technologies without hard templates. Our group reported that large-area and highly ordered arrays are produced by well-developed colloidal lithography techniques [31, 32]. With this method, polymer fluorescent barcode nanorods were generated by the reactive ion etching (RIE) of polymer multilayer films using non-close-packed (ncp) colloidal microsphere arrays as masks [26]. The encoding information of these novel barcode nanorods can easily be tuned by adjusting the thickness and sequences of different fluorescent polymer layers, as well as the number of layers. On the basis of the previous work, we consider whether we can incorporate metal nanoparticles into the polymer segments to achieve encoding.

In this paper, we introduce a versatile method to fabricate Ag nanoparticle/polymer composite barcode nanorods with a high coding capacity. Through layer-by-layer spin-coating, we prepared multilayered alternative thin films of polystyrene (PS) and polyacrylic acid (PAA) on flat substrates. Then, SiO_2 nanosphere monolayers were assembled on the surface of the multilayered films, and RIE was performed to prepare ncp two-dimensional (2D) colloidal crystals, which were used as masks for the following RIE process to fabricate multi-segmented polymer nanorods. Ag nanoparticles were incorporated into the polymer nanorods by an ion exchange and the *in situ* reduction of the Ag^+, and Ag NP/polymer composite barcode nanorods were obtained. The coding capacity can be regulated by increasing the number of segments and changing the thickness and composition of the polymer. The barcode nanorods have potential applications in product tracking and multiplexed biodetection.

2 Experimental

2.1 Preparation of the multi-segmented polymer nanorod arrays

Three-layer films of PAA/PS/PAA were fabricated by sequential spin-coating on a Si/silica substrate, as follows. First, an ethanol solution containing PAA and a 20 mg/mL toluene solution containing PS were

prepared. Both the PAA and the PS were spin-coated at 3,000 rpm for 60 s onto a Si wafer. After each iteration of spin-coating, the polymer film was dried at 130 °C for 10 min to remove the residual solvents. Subsequently, SiO_2 microsphere monolayers were prepared by the interface method. To prepare the ncp 2D colloidal crystals, the RIE of the SiO_2 microsphere monolayers was performed in a gas mixture of CHF_3 at 30 sccm and Ar at 15 sccm. The radiofrequency (RF) power and inductively coupled plasma (ICP) power were 250 and 0 W, respectively. The etching duration was 7 min. Then ncp single-layered colloidal crystals were used as masks for preparing nanorod arrays by the plasma etching of the three-layer polymer films below. Oxygen RIE at a pressure of 10 mTorr, a flow rate of 50 sccm, an RF power of 60 W, and an ICP power of 0 W was performed using a Plasmalab Oxford 80 Plus system. Finally, tri-segmented nanorod arrays were obtained. Five-segmented and seven-segmented polymer nanorod arrays were obtained by similar processes.

2.2 Preparation of the Ag NP/polymer composite nanorods

For the preparation of the Ag nanoparticle/polymer composite nanorod arrays, multi-segmented polymer nanorod arrays were soaked in a 0.3 M aqueous solution of $AgNO_3$ for 12 h and washed with Milli-Q water. The Ag^+ ions that exchanged into the polymer were reduced into Ag NPs by ultraviolet (UV) exposure. For the preparation of the barcode nanorod arrays with an adjustable density, first, four types of solutions were prepared by proportionally mixing PAA and poly(hydroxyethyl methacrylate) (PHEMA): M1, M2, M3, and M5 (containing PAA and PHEMA at volumetric ratios of 1:1, 1:2, 1:3, 1:5, respectively). Four-layered polymer films of PAA/PS/PAA-PHEMA/PS were fabricated onto the Si substrate via repeated spin-coating. Then, multi-segmented nanorod arrays were fabricated using the aforementioned method. The samples were incubated overnight in a $AgNO_3$ aqueous solution at a concentration of 0.3 M and then rinsed with Milli-Q water, followed by the UV-induced reduction of the Ag^+. The nanorods can also be released by soaking them into a corrosive solution to etch away the substrate.

2.3 Characterization

Scanning electron microscopy (SEM) images were obtained using a JEOL Model FESEM 6700F electron microscope with a primary electron energy of 3 kV, and the samples were sputtered with a layer of Pt (~2 nm thick) prior to the imaging to improve the conductivity. The normal absorbance was measured by a collimated beam of a fiber-coupled tungsten-bromine lamp (Ocean Optics), and the spectra were obtained using a spectrometer (Ocean Optics, USB4000) that was operated from 200 to 1,100 nm. The morphology and composition of the nanorods were evaluated by transmission electron microscopy (TEM, Model XL 30 ESEM FEG scanning electron microscope, FEI Company) together with a line scan and elemental mapping in the energy-dispersive X-ray spectroscopy (EDS) mode. Inductively coupled plasma atomic emission spectrometry (ICP-AES) was performed using a PERKIN ELMER OPTIMA 3300DV analyzer.

3 Results and discussion

The overall fabrication process is schematically depicted in Scheme 1. First, polymer multilayers were fabricated by spin-coating. In the optimal case, the solvent for the following layer is a poor solvent for the preceding one. The toluene solution containing PS was chosen because of its incompatibility with the ethanol solution of PAA, as well as its simple preparation method.

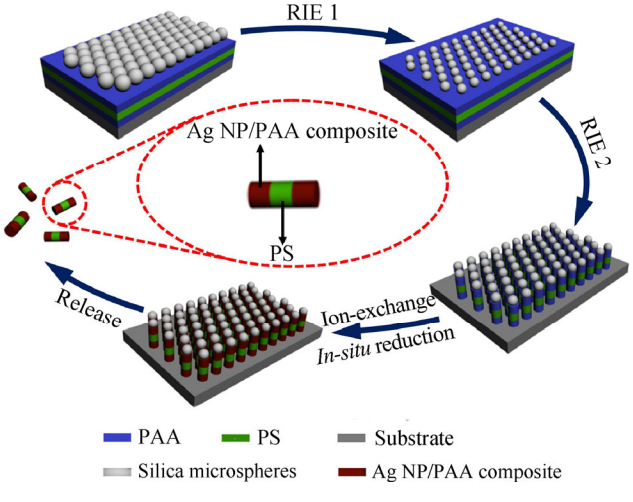

Scheme 1 Schematic of the fabrication procedure for the Ag NP/polymer composite nanorods.

A hexagonal-close-packed (hcp) colloidal monolayer was assembled on an as-prepared substrate by lifting SiO_2 nanospheres at the air/water interface. The hcp SiO_2 colloidal crystal was then etched into an ncp one by RIE, and a sufficient interspace was left for further etching. Subsequently, the exposed polymers were selectively removed by RIE, leaving the nanorods under the microspheres on the substrate. After the Ag NPs were immobilized into the PAA layer by the ion exchange and *in situ* reduction of the Ag^+, the nanorods were released from the substrate by the dissolution of the SiO_2 layer between the substrate and the polymer.

3.1 Preparation of the polymer nanorod arrays

As a typical example, ASA (S = PS, A = PAA) tri-segmented nanorod arrays were fabricated by spin-coating polymer films and performing RIE. Figure 1 shows the morphology of a large-area ncp SiO_2 colloidal crystal. The diameter of the SiO_2 decreased from 800 nm (Fig. 1(a)) to 580 nm (Fig. 1(b)). The SEM images of Figs. 1(c) and 1(d) show a cross-sectional view of the nanorod arrays before and after the removal of the microspheres, respectively. The height of the PAA and PS segments is consistent with that of the PAA and PS polymer films. These results indicate that the HF-etching and cleaning process have no obvious influence on the shape or quality of the nanorods. The PAA and PS segments can be distinguished from the boundary because of the different RIE etching rates of the polymers (the etching rate of the PAA was higher than that of the PS) [26]. Moreover, the top-view SEM images of the oriented nanorod arrays demonstrate the regularity achieved by our method.

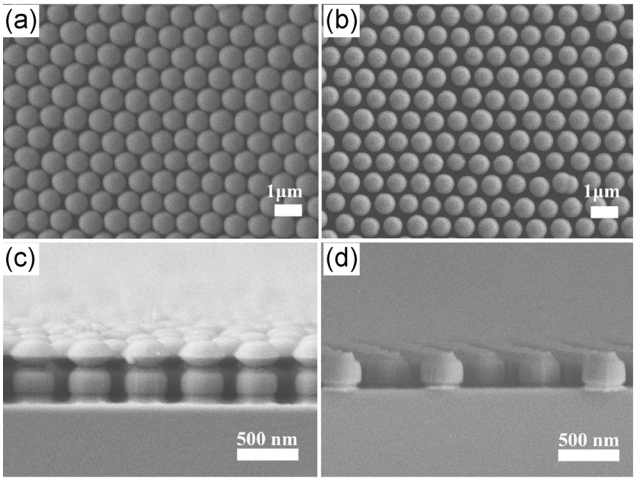

Figure 1 SEM images of the silica nanospheres (a) before and (b) after etching, SEM cross-section images of the polymer nanorod arrays (c) before and (d) after the removal of the silica nanospheres.

3.2 *In situ* preparation of the Ag nanoparticles

The PAA segments were used as matrices for the synthesis of Ag nanoparticles. When the PAA equilibrated in an aqueous solution of $AgNO_3$, the Ag^+ entered the swollen PAA network owing to the ion-exchange with the H^+ in the swollen polymer network. Finally, the Ag NPs were formed by UV exposure [33, 34]. A TEM image shows that the mean diameter of the synthesized Ag NPs in the Ag NP/PAA composite films was ~5 nm (Fig. S1 in the Electronic Supplementary Material (ESM)). In addition, large or partially aggregated particles are clearly visible.

To confirm the presence of the Ag NPs inside the nanorods, we measured the UV-Vis absorption spectra of the nanorods (Fig. 2(a)). As a control experiment, no absorption peak was observed before the deposition of the Ag NPs. However, after the Ag NPs were incorporated into the nanorod array, an absorption band appeared. This absorption band, centered at 430 nm, is attributed to the reduction in the distance between the neighboring Ag NPs in the film compared with the Ag NPs in the aqueous solution [33, 35, 36]. The characteristic peak around the wavelength of 600 nm indicates the presence of large or partially aggregated particles. The inset in Fig. 2(a) shows an optical photograph of the nanorod arrays before and after the immobilization of the Ag NPs. After the chemical attachment of the Ag NPs, the sample changed from colorless to red, which confirms the presence of the Ag NPs in the nanorods.

The nanorods were released by soaking them into a corrosive solution to etch away the substrate. Figures 2(b) and 2(c) show TEM images for different orientations of the Ag NP/polymer composite nanorods. Compared with the nanorod arrays on the substrate, these nanorods exhibited a negligible change in shape after the releasing and cleaning processes. TEM images and the corresponding EDS mapping (Figs. 2(d) and 2(e)) confirm the well-defined distribution of the Ag NPs.

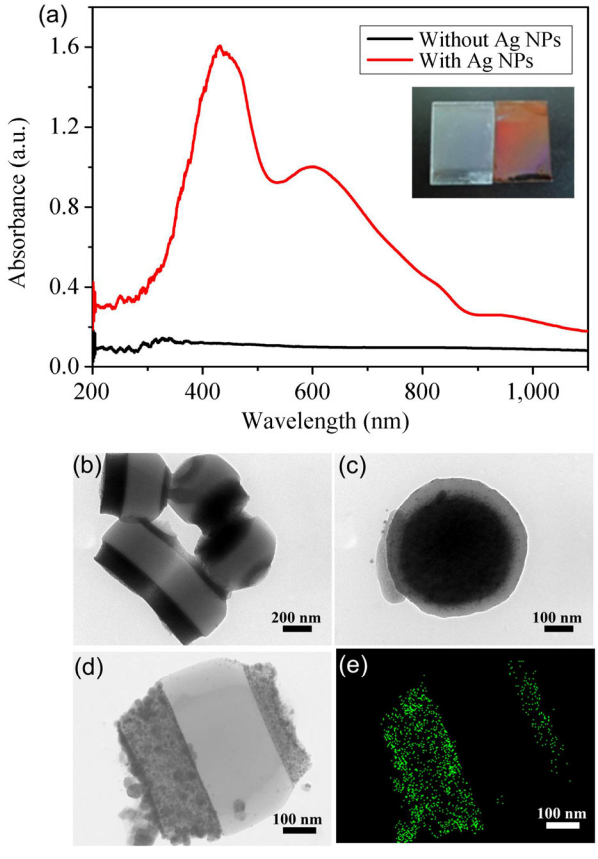

Figure 2 (a) UV absorption spectroscopy of nanorod arrays with and without Ag NPs. (Inset: optical photograph of nanorod arrays before (colorless) and after (red) the immobilization of the Ag NPs). (b) and (c) TEM images of different orientations of the polymer nanorods. (d) TEM image and (e) the corresponding EDS mapping of the tri-segmented Ag NP/polymer nanorod.

3.3 Regulation of the number of nanorod segments

The number of nanorod segments can be easily adjusted by spin-coating alternating layers PAA and PS. For the five-layered and seven-layered polymer films, the morphologies of the multi-segmented nanorod arrays were clearly revealed after the RIE (Figs. 3(a) and 3(b)). In this case, the heights of the PAA and PS segments were 200 and 140 nm, respectively. The Ag NP/polymer composite nanorods were released into water and suspended on a copper grid for TEM imaging (Figs. 3(c) and 3(d)). A well-defined distribution of Ag NPs in the PAA segments was observed.

The etching rate of the PAA was higher than that of the PS. That is, at the same etching time, the diameter of a PS segment was larger than that of a PAA segment (Figs. 3(a) and 3(b)). The different RIE rates

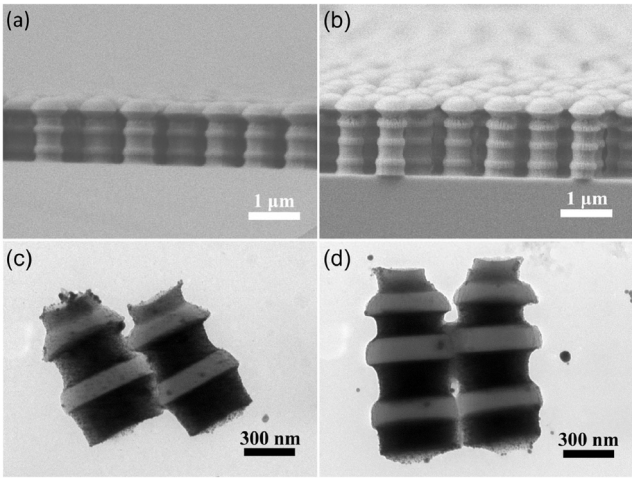

Figure 3 SEM images of the multi-segmented nanorod arrays ((a) and (b)) and the corresponding TEM images ((c) and (d)).

of the two polymers enables shape encoding [26]. We can "write" the code simply by adjusting the bar width.

3.4 Regulation of the length of the PAA segments

In addition to increasing the number of segments, we can change the length of each segment in a single nanorod. The length of the PAA bars is determined by the thickness of the PAA thin films, which can be easily adjusted by tuning the initiative concentrations of the polymer solution and the appropriate etching durations.

Barcode nanorods with different code lengths were prepared by spin-coating the polymers with different concentrations. Multi-segmented nanorods were successfully obtained through a procedure similar to that previously mentioned, while the length of the PAA bar in a single nanorod was different. Figure 4 illustrates the TEM images ((a), (d), and (g)) and the corresponding EDS mapping ((b), (e), and (h)) of the Ag NP/polymer composite nanorods with different PAA thicknesses. The merged images ((c), (f), and (i)) of the TEM images and EDS mappings indicate the well-defined distribution of the Ag NPs in the PAA segments and the increase in the immobilized amount of Ag NPs with the increase in the thickness of the PAA layer. In addition, the sequence of the PAA layers is switchable (see Fig. S2 in the ESM). The controllable length of the nanorods provides opportunities for fabricating accurate multi-segmented barcode nanorods.

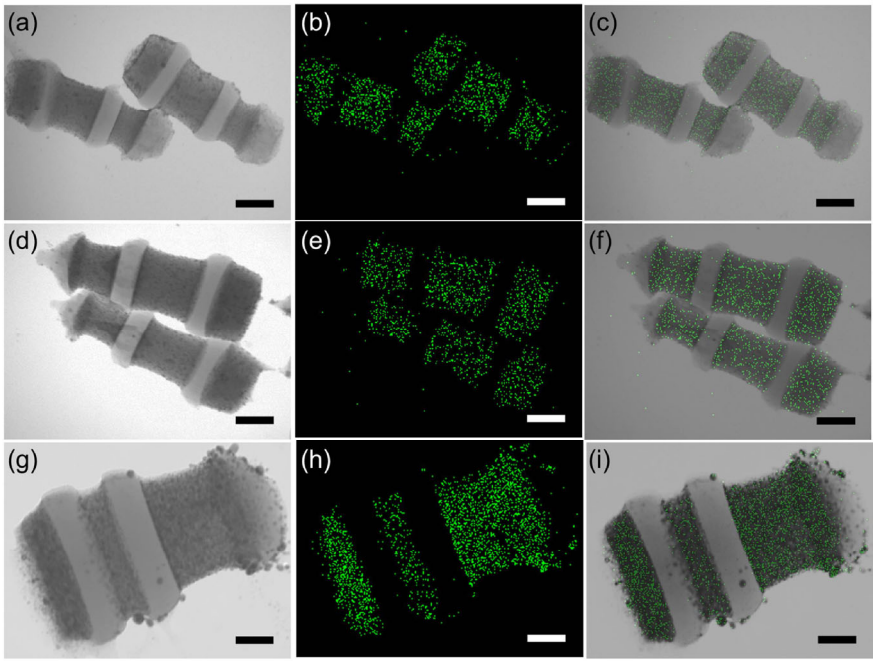

Figure 4 TEM images ((a), (d), and (g)) and the corresponding EDS mapping ((b), (e), and (h)) of Ag NP/polymer barcode nanorods with different PAA length. (c), (f), and (i) are the merged images of TEM images and EDS mappings. In (a), (d), and (g), the length ratios of PAA bars (bottom to top) are 1:2:1, 4:6:5 and 1.5:1:4, respectively. Scale bars: 200 nm.

3.5 Regulation of the density of the Ag NPs

The differences in the density of the Ag NPs can also increase the coding capacity of the barcode nanorods. During the incorporation of the Ag NPs into the polymer segments, the density of the Ag NPs was regulated by tuning the composition of the polymer solution in each layer. We can finely regulate Ag NPs by physically blending PHEMA and PAA, as PHEMA is mixable with PAA but cannot conduct the Ag^+ exchange process. This means that a PAA layer mixed with PHEMA absorbs less Ag^+ than one without PHEMA. To confirm the content of the Ag NPs in the composite, the fabrication process was performed for a PAA-PHEMA polymer thin film. Thin films with different compositions were fabricated by spin-coating onto a silica substrate. Then, the polymer thin films were soaked in a $AgNO_3$ aqueous solution, and the Ag^+ was reduced to Ag NPs by UV exposure. Figure 5(a) shows the UV absorption spectra, where the appearance of a single peak around 430 nm indicates the existence of the Ag NPs [37]. The intensity of the absorption peak clearly decreased as the PHEMA content increased.

These results reveal a decrease in the immobilized amount of Ag NPs as the PHEMA content increased. To confirm the presence of the Ag NPs in the polymer, an EDS elemental analysis was performed on the samples (Fig. 5(b)). The appearance of Ag signals strongly confirmed the presence of the Ag NPs in the polymer film. In addition, to determine the atomic ratio of Ag, we performed an ICP test. The samples were dissolved in HNO_3, and the ICP results revealed a decrease in the immobilized amount of Ag NPs as the volume fraction of PHEMA increased. According to these data, the atomic concentrations of Ag are estimated as 1.70%, 0.77%, 0.50%, 0.21%, and 0.15% for the different samples, as shown in Table 1.

On the basis of the fabricated ASAS nanorods, polymer films with different PAA-PHEMA compositions were generated by repeated spin-coating onto silica substrates. Then, multi-segmented nanorod arrays were clearly observed through a similar process. The TEM images and the corresponding EDS mapping (Figs. 6(a)–6(h)) show the well-maintained morphology and well-defined distribution of the Ag NPs. From the EDS mapping, we observe that the PAA-PHEMA gray segments were a few shades lighter than the PAA segments, which indicates that the content of Ag

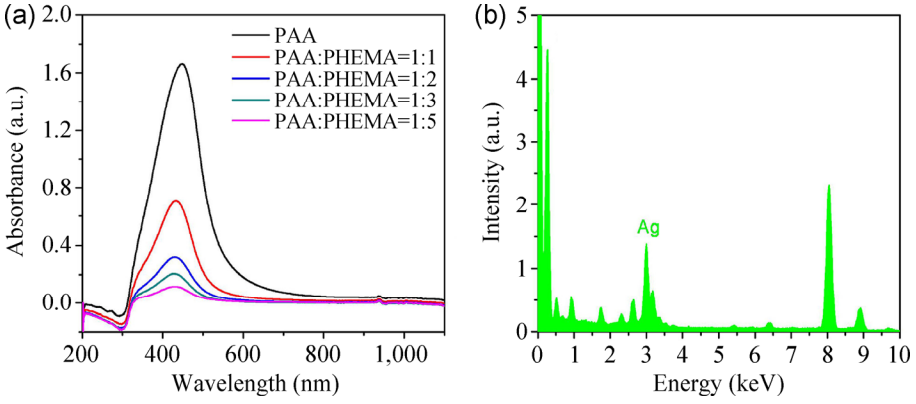

Figure 5 (a) UV-Vis spectra of different polymer films containing Ag NPs. (b) EDS elemental analysis of Ag.

Table 1 Atomic concentrations of Ag in different polymer films

Polymer composition	ω_{Ag} (%)
PAA	1.70
M1 (PAA:PHEMA=1:1)	0.77
M2 (PAA:PHEMA=1:2)	0.50
M3 (PAA:PHEMA=1:3)	0.21
M5 (PAA:PHEMA=1:5)	0.15

NPs in the PAA-PHEMA layer was less than that in the PAA layer. Elemental line scanning (Figs. 6(i)–6(l)) of Ag along the nanorods also revealed the different polymer segments with different intensity ratios. We calculated the integral areas of the intensities of the Ag elements in the PAA segments and PAA-PHEMA segments. As shown in Fig. 6(i), the intensity ratio of the Ag in the PAA segment to that in the PAA:PHEMA = 1:1 segment was 1:0.56. Similarly, the intensity ratios shown in Figs. 6(j)–6(l) are 1:0.53, 1:0.50, and 1:0.35, respectively. The data indicate that the intensity decreased as the volume fraction of PHEMA increased; that is, the immobilized amount of Ag NPs decreased as the volume fraction of PHEMA increased.

The introduction of the polymers with different compositions not only enhanced the gray contrast of the nanorods but also expanded the scope of the coding. We demonstrated the use of the nanorods as barcodes. The barcode nanorods displayed different optical properties. We measured the UV–Vis spectra (Fig. 7) of nanorod arrays prepared with different polymer compositions. The peak intensity increased as the Ag concentration (volume fraction of the PAA) increased, and it was highest for the PAA/PS/M1/PS nanorod. In addition, the films exhibited a high wavelength shoulder at the resonance peak and an increase in the intensity of the absorbance band around 800 nm as the volume fraction of PHEMA was increased. The resonance peak broadened because the Ag NPs size distribution broadened. As is widely known, the size and shape of NPs determine the characteristics of the plasmon resonance. As the diameter of the spherical particles increases, the plasmon resonance shifts toward longer wavelengths (i.e., redshift). However, the plasmon resonance peak can also shift toward longer wavelengths if the NP shape changes from a sphere to a cube (or pentagon or triangle). The peak at 459 nm is consistent with spherical NPs and was characterized by TEM. Regarding the peak at 800 nm, we speculate that immobilized particles were present in the form of domains, as the PAA phase and PHEMA phase were present on the PAA-PHEMA polymer layer, but the Ag NPs existed only in the PAA phase. In this case, the absorption characteristics of the formed Ag NPs may indicate the presence of larger or non-spherical particles [38]. Remarkably, the spectra reveal that different nanorods can provide different optical signals. The barcode nanorods have potential applications in product tracking and multiplexed biodetection.

We attempted to verify the stability of the barcode nanorods using their structure and optical properties. After 30 days, the nanorod structures remained stable whether the nanorods were in the solution or in air, and the absorption spectra of the nanorods exhibited almost no change.

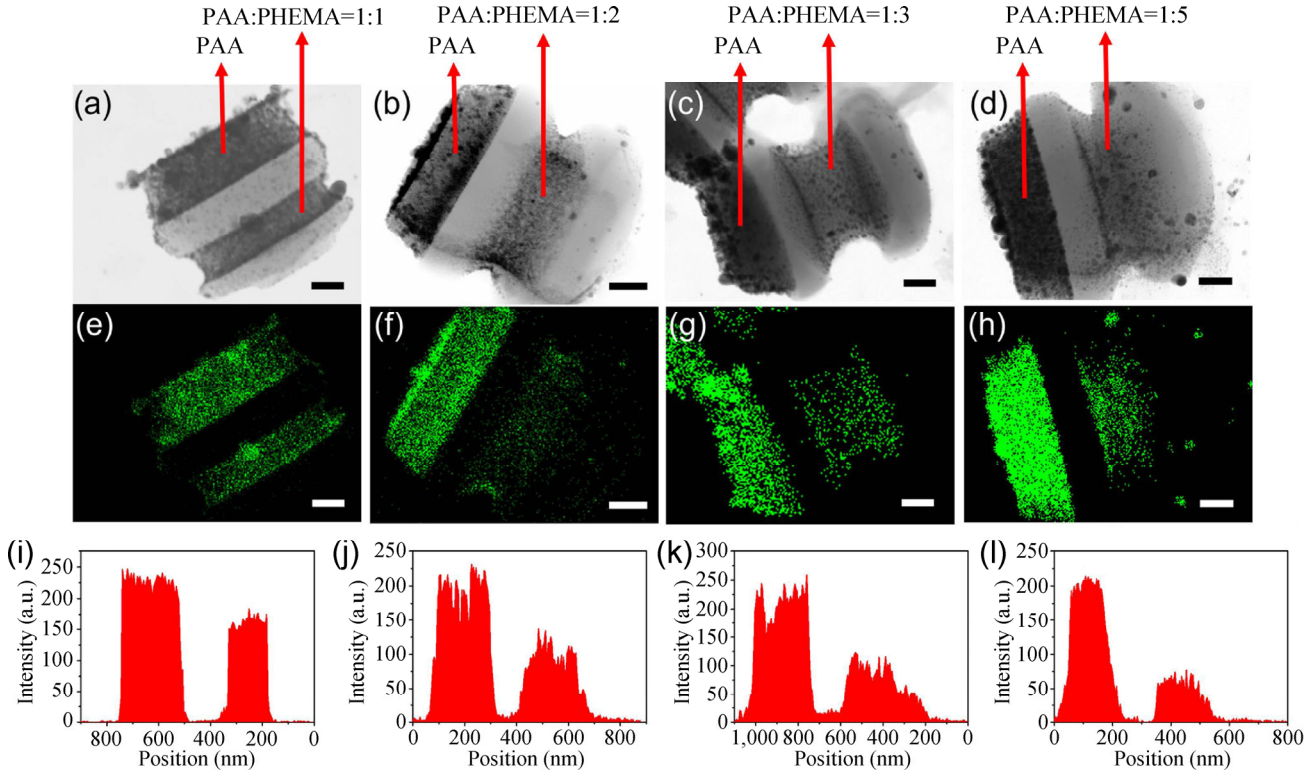

Figure 6 (a)–(d) TEM images of barcode nanorods and (e)–(h) the corresponding EDS mapping. (i)–(l) Elemental line scanning of barcode nanorods. Scale bars: 100 nm.

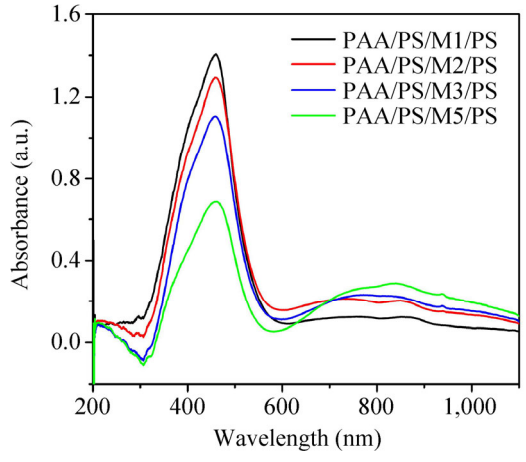

Figure 7 UV-absorption spectroscopy of Ag NPs-doped barcode nanorod arrays with different polymer compositions.

The key advantage of our method is the intrinsic simplicity of the delicate control of the Ag NP content. We confirmed the tunability by fabricating additional nanorod segments. As shown in Fig. S3 (in the ESM), an addition coding scheme was produced. The approximate profiles of the pattern were successfully reproduced after releasing. This result further verifies the flexibility of our method for fabricating barcode nanorods.

4 Conclusions

We demonstrated a versatile approach to generate barcode nanorods with a controlled coding capacity. The encoding information of these novel barcode nanorods was easily tuned by adjusting the number of segments, the length of the PAA bars, and the density of the Ag NPs. By changing the Ag NP content, the absorbance spectra of the barcode nanorods was adjusted. Moreover, the barcode nanorods were easily detached from the substrates to form a dispersion of coding materials. Considering their simple and low-cost fabrication, these encoding nanorods have a wide range of potential applications in product tracking and multiplexed biodetection. Furthermore, we believe that numerous coded materials can be obtained by introducing other functional nanoparticles into the structure of the nanorods. This introduces new approaches for fabricating barcoded nanomaterials.

Acknowledgements

This work was supported by the National Basic Research Program of China (No. 2012CB933800), the National Natural Science Foundation of China (No. 21222406, 21474037, 91123031, and 21221063), the Program for New Century Excellent Talents in University, Doctoral Fund of Ministry of Education of China (No. 20130061110019), and Science and Technology Development Program of Jilin Province.

Electronic Supplementary Material: Supplementary material (chemicals and materials, supplementary figures) is available in the online version of this article at http://dx.doi.org/ 10.1007/s12274-015-0792-0.

References

[1] Huang, X. N.; Huang, G.; Zhang, S. R.; Sagiyama, K.; Togao, O.; Ma, X. P.; Wang, Y. G.; Li, Y.; Soesbe, T. C.; Sumer, B. D. et al. Multi-chromatic pH-activatable ^{19}F-MRI nanoprobes with binary ON/OFF pH transitions and chemical-shift barcodes. *Angew. Chem., Int. Ed.* **2013**, *52*, 8074–8078.

[2] Wilson, R.; Cossins, A. R.; Spiller, D. G. Encoded microcarriers for high-throughput multiplexed detection. *Angew. Chem., Int. Ed.* **2006**, *45*, 6104–6017.

[3] Finkel, N. H.; Lou, X. H.; Wang, C. Y.; He, L. Barcoding the microworld. *Anal. Chem.* **2004**, *76*, 352A–359A.

[4] Han, M. Y.; Gao, X. H.; Su, J. Z.; Nie, S. M. Quantum-dot-tagged microbeads for multiplexed optical coding of biomolecules. *Nat. Biotechnol.* **2001**, *19*, 631–635.

[5] Pregibon, D. C.; Toner, M.; Doyle, P. S. Multifunctional encoded particles for high-throughput biomolecule analysis. *Science* **2007**, *315*, 1393–1396.

[6] Gershon, D. Microarray technology: An array of opportunities. *Nature* **2002**, *416*, 885–891.

[7] Nicewarner-Peña, S. R.; Freeman, R. G.; Reiss, B. D.; He, L.; Peña, D. J.; Walton, I. D.; Cromer, R.; Keating, C. D.; Natan, M. J. Submicrometer metallic barcodes. *Science* **2001**, *294*, 137–141.

[8] Birtwell, S.; Morgan, H. Microparticle encoding technologies for high-throughput multiplexed suspension assays. *Integr. Biol.* **2009**, *1*, 345–362.

[9] Banholzer, M. J.; Millstone, J. E.; Qin, L. D.; Mirkin, C. A. Rationally designed nanostructures for surface-enhanced Raman spectroscopy. *Chem. Soc. Rev.* **2008**, *37*, 885–897.

[10] Zhang, Y.; Wang, H.; Nie, J. F.; Zhou, H.; Shen, G. L.; Yu, R. Q. Mussel-inspired fabrication of encoded polymer films for electrochemical identification. *Electrochem. Commun.* **2009**, *11*, 1936–1939.

[11] Stoermer, R. L.; Cederquist, K. B.; McFarland, S. K.; Sha, M. Y.; Penn, S. G.; Keating, C. D. Coupling molecular beacons to barcoded metal nanowires for multiplexed, sealed chamber DNA bioassays. *J. Am. Chem. Soc.* **2006**, *128*, 16892–16903.

[12] Qin, L. D.; Banholzer, M. J.; Millstone, J. E.; Mirkin, C. A. Nanodisk codes. *Nano Lett.* **2007**, *7*, 3849–3853.

[13] Nam, J. M.; Thaxton, C. S.; Mirkin, C. A. Nanoparticle-based bio-barcodes for the ultrasensitive detection of proteins. *Science* **2003**, *301*, 1884–1886.

[14] Tok, J. B.-H.; Chuang, F. Y. S.; Kao, M. C.; Rose, K. A.; Pannu, S. S.; Sha, M. Y.; Chakarova, G.; Penn, S. G.; Dougherty, G. M. Metallic striped nanowires as multiplexed immunoassay platforms for pathogen detection. *Angew. Chem., Int. Ed.* **2006**, *45*, 6900–6904.

[15] Eastman, P. S.; Ruan, W. M.; Doctolero, M.; Nuttall, R.; de Feo, G.; Park, J. S.; Chu, J. S. F.; Cooke, P.; Gray, J. W.; Li, S. et al. Qdot nanobarcodes for multiplexed gene expression analysis. *Nano Lett.* **2006**, *6*, 1059–1064.

[16] Wang, J. Barcoded metal nanowires. *J. Mater. Chem.* **2008**, *18*, 4017–4020.

[17] Zhao, Y. J.; Shum, H. C.; Chen, H. S.; Adams, L. L. A.; Gu, Z. Z.; Weitz, D. A. Microfluidic generation of multifunctional quantum dot barcode particles. *J. Am. Chem. Soc.* **2011**, *133*, 8790–8793.

[18] Seo, D.; Yoo, C. I.; Jung, J.; Song, H. Ag-Au-Ag heterometallic nanorods formed through directed anisotropic growth. *J. Am. Chem. Soc.* **2008**, *130*, 2940–2941.

[19] Rauf, S.; Glidle, A.; Cooper, J. M. Production of quantum dot barcodes using biological self-assembly. *Adv. Mater.* **2009**, *21*, 4020–4024.

[20] Battersby, B. J.; Bryant, D.; Meutermans, W.; Matthews, D.; Smythe, M. L.; Trau, M. Toward larger chemical libraries: Encoding with fluorescent colloids in combinatorial chemistry. *J. Am. Chem. Soc.* **2000**, *122*, 2138–2139.

[21] Kuang, M.; Wang, D. Y.; Bao, H. B.; Gao, M. Y.; Möhwald, H.; Jiang, M. Fabrication of multicolor-encoded microspheres by tagging semiconductor nanocrystals to hydrogel spheres. *Adv. Mater.* **2005**, *17*, 267–270.

[22] Dejneka, M. J.; Streltsov, A.; Pal, S.; Frutos, A. G.; Powell, C. L.; Yost, K.; Yuen, P. K.; Müller, U.; Lahiri, J. Rare earth-doped glass microbarcodes. *Proc. Natl. Acad. Sci. USA* **2003**, *100*, 389–393.

[23] Hurst, S. J.; Payne, E. K.; Qin, L. D.; Mirkin, C. A. Multisegmented one-dimensional nanorods prepared by hard-template synthetic methods. *Angew. Chem., Int. Ed.* **2006**, *45*, 2672–2692.

[24] Sattayasamitsathit, S.; Burdick, J.; Bash, R.; Kanatharana,

P.; Thavarungkul, P.; Wang, J. Alloy nanowires barcodes based on nondestructive X-ray fluorescence readout. *Anal. Chem.* **2007**, *79*, 7571–7575.

[25] Wanekaya, A. K.; Chen, W.; Myung, N. V.; Mulchandani, A. Nanowire-based electrochemical biosensors. *Electroanalysis* **2006**, *18*, 533–550.

[26] Li, X.; Wang, T. Q.; Zhang, J. H.; Zhu, D. F.; Zhang, X.; Ning, Y.; Zhang, H.; Yang, B. Controlled fabrication of fluorescent barcode nanorods. *ACS Nano* **2010**, *4*, 4350–4360.

[27] Zhao, Y. J.; Cheng, Y.; Shang, L. R.; Wang, J.; Xie, Z. Y.; Gu, Z. Z. Microfluidic synthesis of barcode particles for multiplex assays. *Small* **2015**, *11*, 151–174.

[28] Zhang, Y. H.; Zhang, L. X.; Deng, R. R.; Tian, J.; Zong, Y.; Jin, D. Y.; Liu, X. G. Multicolor barcoding in a single upconversion crystal. *J. Am. Chem. Soc.* **2014**, *136*, 4893–4896.

[29] Mirkin, C. A.; Letsinger, R. L.; Mucic, R. C.; Storhoff, J. J. A DNA-based method for rationally assembling nanoparticles into macroscopic materials. *Nature* **1996**, *382*, 607–609.

[30] Service, R. F. Solar energy. Can the upstarts top silicon? *Science* **2008**, *319*, 718–720.

[31] Zhang, J. H.; Li, Y. F.; Zhang, X. M.; Yang, B. Colloidal self-assembly meets nanofabrication: From two-dimensional colloidal crystals to nanostructure arrays. *Adv. Mater.* **2010**, *22*, 4249–4269.

[32] Zhang, J. H.; Yang, B. Patterning colloidal crystals and nanostructure arrays by soft lithography. *Adv. Funct. Mater.* **2010**, *20*, 3411–3424.

[33] Kim, Y. W.; Lee, D. K.; Lee, K. J.; Min, B. R.; Kim, J. H. *In situ* formation of silver nanoparticles within an amphiphilic graft copolymer film. *J. Polym. Sci., Part B: Polym. Phys.* **2007**, *45*, 1283–1290.

[34] Chen, M. J.; Zhao, Y. N.; Yang, W. T.; Yin, M. Z. UV-irradiation-induced templated/*in-situ* formation of ultrafine silver/polymer hybrid nanoparticles as antibacterial. *Langmuir* **2013**, *29*, 16018–16024.

[35] Cocca, M.; D'Orazio, L. Novel silver/polyurethane nanocomposite by *in situ* reduction: Effects of the silver nanoparticles on phase and viscoelastic behavior. *J. Polym. Sci., Part B: Polym. Phys.* **2008**, *46*, 344–350.

[36] Gupta, S.; Uhlmann, P.; Agrawal, M.; Chapuis, S.; Oertel, U.; Stamm, M. Immobilization of silver nanoparticles on responsive polymer brushes. *Macromolecules* **2008**, *41*, 2874–2879.

[37] Henglein, A.; Giersig, M. Formation of colloidal silver nanoparticles: Capping action of citrate. *J. Phys. Chem. B* **1999**, *103*, 9533–9539.

[38] Deshmukh, R. D.; Composto, R. J. Surface segregation and formation of silver nanoparticles created in situ in poly(methyl methacrylate) films. *Chem. Mater.* **2007**, *19*, 745–754.